PHYSICAL REVIEW C VOLUME 24, NUMBER 2 AUGUST 1981

Pion inelastic scattering to the low-lying states in ^{42,44,48}Ca: Determination of the neutron and proton multipole matrix elements

Kenneth G. Boyer,* William B. Cottingame,† L. E. Smith, Steven J. Greene,† and C. Fred Moore
University of Texas at Austin, Austin, Texas 78712

J. S. McCarthy, R. C. Minehart, and J. F. Davis‡
University of Virginia, Charlottesville, Virginia 22904

G. R. Burleson and G. Blanpied§
New Mexico State University, Las Cruces, New Mexico 88003

Chuck A. Goulding‖
Florida A & M University, Tallahassee, Florida 32307

Henry A. Thiessen and Christopher L. Morris
Los Alamos National Laboratory, Los Alamos, New Mexico 87545
(Received 19 January 1981)

A distorted-wave impulse-approximation analysis of 180-MeV $\pi^{\pm}$ inelastic-scattering data to the 2_1^+ and 3_1^- states in ^{42,44,48}Ca is used to extract the neutron and proton (alternatively, isovector and isoscalar) multipole matrix elements for exciting these states. Model-dependent errors are examined by comparing results of calculations using collective-model form factors with those using form factors fitted to electron inelastic-scattering data.

[NUCLEAR REACTIONS ^{42,44,48}Ca($\pi^{\pm}, \pi^{\pm}$); measured $\sigma(\theta)$; DWIA analysis; deduced neutron and proton multipole matrix elements.]

I. INTRODUCTION

Multipole matrix elements from model-dependent analyses of hadron inelastic scattering [such as (α, α') (Ref. 1) and (p, p') (Ref. 2)] have been compared with measured electromagnetic matrix elements $M(E\lambda)$ from lifetime, gamma-ray linewidth or Coulomb excitation measurements to obtain the ratios of the neutron $M(n\lambda)$ to proton $M(p\lambda)$ multipole matrix elements for low-lying collective states in many single closed-shell nuclei. Because of the unique signatures of valence-particle excitations (either pure neutron or pure proton) and of core excitations (N/Z admixtures of neutron and proton) in single closed-shell nuclei, such studies offer the possibility of understanding core-polarization effects. However, these comparisons are limited, as shown by analyses of inelastic electron scattering, where the interaction is well known; different models for the transition densities give equally good fits to the measured form factors but give different values for the electromagnetic matrix elements.[3,4] In the case of hadronic probes, where the interaction is not well known, model-dependent errors might be expected to be larger.

Comparisons of inelastic scattering of hadronic probes existing in isotopic multiplets, e.g., (n,n') and (p,p') (Ref. 5) *or* $(\pi^+, \pi^{+\prime})$ and $(\pi^-, \pi^{-\prime})$,[6] have been suggested as a method for obtaining $M(n\lambda)$ and $M(p\lambda)$ that avoids some model-dependent errors. If the relative strengths of the isovector and isoscalar parts of the force are understood, most of the model-dependent errors should be contained in the value of the matrix elements and should cancel in ratios such as $M(n\lambda)/M(p\lambda)$.

A previous study[7] of pion inelastic scattering from the self-conjugate ($N = Z$) nuclei ^{12}C and ^{40}Ca showed that pure isoscalar transition densities obtained from inelastic electron scattering gave equally good fits to both π^+ and π^- inelastic scattering with no adjustable parameters. The current distorted-wave impulse-approximation (DWIA) analysis of inelastic scattering to the low-lying collective states in the $N \neq Z$ single closed-shell nuclei ^{42,44,48}Ca uses both collective-model form factors and more "microscopic" form factors fitted to electron inelastic scattering. Both neutron and proton multipole matrix elements are deduced, and model-dependent errors are examined.

II. DATA ACQUISITION

Data were obtained using the Energetic Pion Channel and Spectrometer (EPICS) system at the Los Alamos Clinton P. Anderson Meson Physics Facility (LAMPF). The EPICS system, described

in Ref. 8, consists of a momentum-dispersing channel and a high-resolution spectrometer. Position-sensitive, delay-line read-out drift chambers measure the particle trajectories, that is, positions and angles, both before and after the spectrometer dipoles. For each event, an on-line computer program projects the trajectory back to the scattering target to reconstruct the scattering angle and incident momentum; the scattered pion momentum is calculated to third order in the particle coordinates. A Q value for the reaction is calculated and histogrammed using these momenta and the scattering angle.

Data were obtained with a channel momentum bite of ±2%. The pion flux (approximately 10^8 π^+/s and 2×10^7 π^-/s) was monitored by two ion chambers 75 cm downstream of the target. The ion chambers had a 1-cm-thick iron absorber between them to range out incident protons, providing a monitor of the incident pion beam and of proton contamination. The angular resolution of the beam was about 10 mrad.

Data were taken with a reduced spectrometer acceptance of 8 msr. The scattering-angle acceptance was ±1.5°; the momentum acceptance of the spectrometer was ±6%, which allowed a 30-MeV region of excitation energy to be studied in one setting. This was large enough to require only one spectrometer setting for all angle settings.

Five isotopically enriched 4-cm-high target strips were simultaneously mounted in the 20-cm-high pion beam. Software gates on the target position calculated for each scattered pion (3-mm resolution) separated interactions in the different target strips. The strips were arranged so that, by shifting the target ladder, each strip could be replaced by ^{40}Ca. The reproducibility of the ^{40}Ca results (±2%) was an indication of the size of systematic errors arising from changes in the beam intensity or the spectrometer solid angle as a function of target position. Relative cross sections between the isotopes are accurate to the same level (±2%).

Typical spectra obtained for pion scattering from ^{40,42,44,48}Ca are presented in Fig. 1. Data are given for the (2^+_1, 1.52-MeV) and (3^-_1, 3.45-MeV) states in ^{42}Ca; the (2^+_1, 1.16-MeV) and (3^-_1, 3.31-MeV) states in ^{44}Ca; and the (2^+_1, 3.83-MeV)

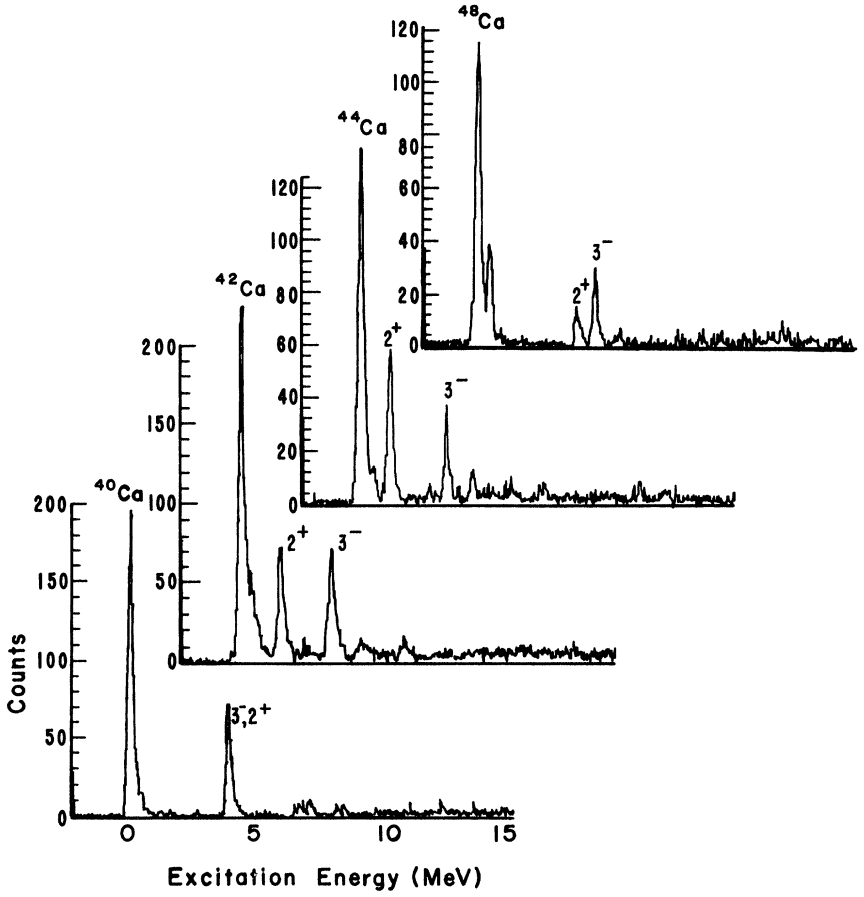

FIG. 1. Typical pion energy-loss spectra.

and (3_1^-, 4.50-MeV) states in ^{48}Ca. All data were taken at an incident pion energy of 180 MeV at laboratory angles between 21° and 76°.

III. DATA REDUCTION

Peak areas, extracted from the Q-value spectra using the program LOAF,[9] were fitted with a fixed line shape extracted from the elastic-scattering peak. Relative separations between peaks were constrained at values obtained from the energy-level compilations.[10]

The data were normalized to π^+ and π^- scattering on hydrogen, using the Coulomb-corrected phase shifts of Rowe *et al.*[11] The ratio of experimental yield to the predicted $\pi^+ + p$ cross sections was flat to within ±5% in the angular region between 40° and 90°. The data were corrected for solid angle as a function of position along the focal plane, survival fraction through the spectrometer, chamber efficiency, and computer live time. The correction for solid angle was measured by mapping the focal plane using elastic scattering from natural iron at an angle of 38°, which corresponds to the first maximum in its angular distribution. Chamber efficiency and computer live times were monitored on line.

Estimated systematic errors in the data set include: normalization error, ±3%; focal-plane variation of solid angle, ±2%; peak-shape fitting errors, ±5%; survival fraction correction, ±3%; chamber efficiency, ±3%; and beam monitoring, ±3%. The overall normalization uncertainty was ±9%, with a relative π^+ vs π^- uncertainty of ±6%. Because of count-rate variations, the chamber efficiencies are a function of angle, and systematic angle-dependent errors of ±5% may occur.

At each angle the elastic-scattering data have been corrected to remove a change in the momentum transfer [$q = 2k\sin(\theta/2)$] that arises because of the momentum dispersion of the incident beam. The center of mass scattering angle was transformed by

$$\sin(\theta'/2) = \frac{\sin(\theta/2)}{1 + x/d}\ , \tag{1}$$

where θ is the scattering angle, x is the target position relative to the center of the beam, d is the momentum dispersion of the channel (10 cm/%), and θ' is the corrected angle. This correction deepened the minima in the elastic-scattering angular distributions. It was not applied to the inelastic-scattering data.

A significant oxygen contaminant in the calcium targets was subtracted by fitting both elastic-scattering peaks separately at all angles greater than 24°. The only known contaminant in the inelastic-scattering data resulted from a 5% ^{40}Ca content in the ^{48}Ca target. Consequently, contributions from the (3^-, 3.73-MeV) state in ^{40}Ca were subtracted from the yield for the (2^+, 3.83-MeV) state in ^{48}Ca.

IV. ELASTIC-SCATTERING ANALYSIS

The coordinate-space computer code DWPI (Ref. 12) was used for both elastic and inelastic DWIA calculations. All calculations used the Kisslinger[13] form for the optical-model potential,

$$V(r) = b_{00}k_\pi^{\,2}\rho_0(r) + b_{10}\vec{\nabla}\cdot\rho_0(r)\vec{\nabla} - \epsilon_\pi[b_{01}k_\pi^{\,2}\rho_1(r) + b_{11}\vec{\nabla}\cdot\rho_1(r)\vec{\nabla}]\,, \tag{2}$$

where $\rho_0(r)$ is the isoscalar density distribution $[N\rho_n(r) + Z\rho_p(r)]/A$, and $\rho_1(r)$ is the isovector density distribution $[N\rho_n(r) - Z\rho_p(r)]/A$. Here, b_{00}, b_{01}, and b_{11} are related to the π-nucleon scattering amplitudes, k_π is the pion momentum, and ϵ_π is the sign of the pion charge. The b coefficients were evaluated using the method in Ref. 14 with a negative energy shift of 30 MeV. The results are

$$b_{00} = -0.59 + 0.30i\,,$$
$$b_{01} = -0.99 + 0.03i\,,$$
$$b_{10} = 4.38 + 7.19i\,, \tag{3}$$

and

$$b_{11} = 2.46 + 3.59i\,.$$

TABLE I. Ground-state density-distribution parameters.

Nucleus	c_p (fm)	a_p (fm)	c_n (fm)	a_n (fm)	$\langle r^2\rangle_p^{1/2}$ (fm)	$\langle r^2\rangle_n^{1/2}$ (fm)
^{42}Ca	3.52	0.55	3.46	0.55	3.41	3.37
^{44}Ca	3.52	0.55	3.52	0.55	3.41	3.41
^{48}Ca	3.46	0.55	3.63	0.55	3.37	3.48

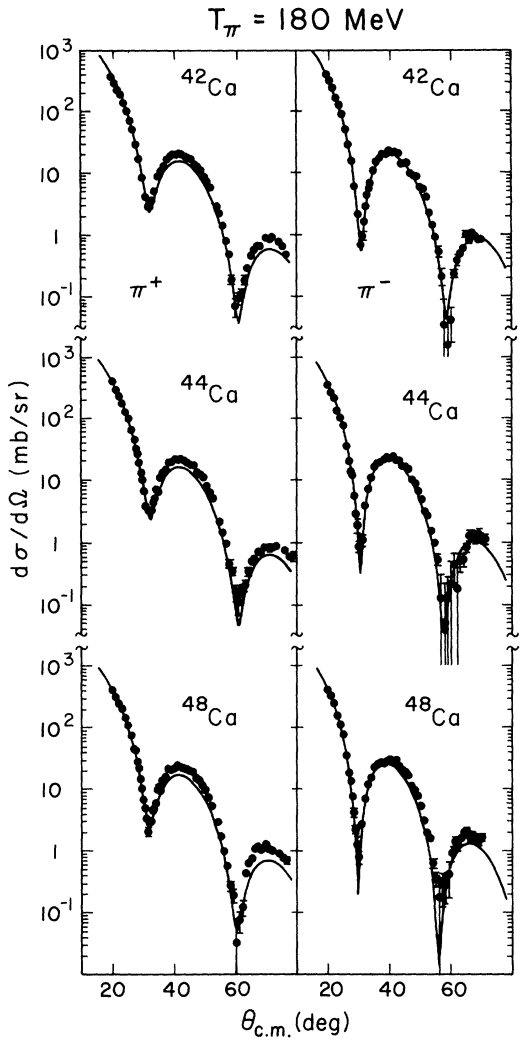

FIG. 2. Elastic-scattering fits and data.

Both the neutron and proton distributions were parametrized with a Woods-Saxon distribution,

$$\rho(r) = \rho_0\{1+\exp[(r-c)/a]\}^{-1}. \quad (4)$$

The diffusivity a was fixed at 0.55 fm for all distributions. For the proton distributions, the half-density radii c_p were adjusted to reproduce the rms radius of the point proton distribution, which was obtained by unfolding the proton charge distribution from the charge distributions measured in elastic electron scattering.[15] The neutron parameter c_n was adjusted to reproduce the location of the first minimum in the π^- angular distribution. The resulting parameters are listed in Table I. The data and resulting fits are shown in Fig. 2.

V. INELASTIC-SCATTERING ANALYSIS

Both collective-model form factors and more microscopic form factors obtained from fitting electron-scattering data were used to analyze the inelastic data. For the microscopic-model calculations, both the neutron and proton transition densities had the same radial shapes and were given by the models used in fitting the electron-scattering data (a Gaussian model[4] for ^{42,44}Ca and a Tassie model[16] for ^{48}Ca). The radial shapes of the transition densities in the collective-model calculations (given by the derivatives of ground-state density distributions) differed. The ground-state densities used are those given in Table I. Strength parameters $\beta_n(\beta_p)$ for the neutron (proton) distributions were adjusted to fit the forward part of the angular distributions. Neutron $M(n\lambda)$ and proton $M(p\lambda)$ reduced multipole matrix elements were then calculated from the transition densities $\rho_{tr,n}(r)$ and $\rho_{tr,p}(r)$, as in Ref. 17

$$M(n\lambda) = \int_0^\infty r^{\lambda+2}\rho_{tr,n}(r)dr\,,$$
$$M(p\lambda) = \int_0^\infty r^{\lambda+2}\rho_{tr,p}(r)dr\,. \quad (5)$$

Isoscalar and isovector matrix elements are

$$M(0\lambda) = \tfrac{1}{2}[M(n\lambda)+M(p\lambda)]\,,$$
$$M(1\lambda) = \tfrac{1}{2}[M(n\lambda)-M(p\lambda)]\,. \quad (6)$$

In the long-wavelength limit, these matrix elements (listed in Tables II and III) are related to the electromagnetic transition rates by

$$B(E_\lambda, J_i \to J_f) = |M(p\lambda)|^2/(2J_i+1)\,. \quad (7)$$

TABLE II. Neutron and proton multipole matrix elements for the 2^+ states. The symbols n, p, and E denote neutron, proton, and electromagnetic. All matrix elements are in Weisskopf single-particle units.

Nucleus	Microscopic model $M(n2)$	Microscopic model $M(p2)$	Microscopic model $\frac{M(n2)}{M(p2)}$	Collective model $M(n2)$	Collective model $M(p2)$	Collective model $\frac{M(n2)}{M(p2)}$	$M(E2)$[a]
^{42}Ca	3.22(22)	2.80(21)	1.15(14)	3.54(24)	2.93(22)	1.21(15)	3.08(10)
^{44}Ca	3.50(23)	2.87(22)	1.22(15)	3.98(26)	3.04(23)	1.31(16)	3.13(11)
^{48}Ca	3.60(21)	1.37(15)	2.63(37)	3.71(22)	1.56(16)	2.38(33)	1.48(10)

[a]The electromagnetic matrix elements were obtained from Ref. 18.

TABLE III. Neutron and proton multipole matrix elements for the 3^- states. The symbols n, p, and E denote neutron, proton, and electromagnetic. All matrix elements are in Weisskopf single-particle units.

Nucleus	Microscopic model $M(n3)$	$M(p3)$	$\frac{M(n3)}{M(p3)}$	Collective model $M(n3)$	$M(p3)$	$\frac{M(n3)}{M(p3)}$	$M(E3)$[a]
^{42}Ca	3.59(27)	4.06(28)	0.88(11)	3.95(29)	4.41(30)	0.89(11)	
^{44}Ca	2.93(21)	3.10(22)	0.94(11)	3.21(23)	3.44(24)	0.93(11)	
^{48}Ca	3.70(25)	3.17(24)	1.17(14)	3.57(25)	3.13(23)	1.14(14)	2.59(39)

[a]The electromagnetic matrix elements were obtained from Ref. 18.

The data and fits for the collective and microscopic models are shown in Figs. 3 and 4.

VI. RESULTS

The matrix elements, and especially the ratios $R = M(n\lambda)/M(p\lambda)$, obtained from the calculations using the two models for the form factors (Tables II and III) are in good agreement. Further, the results for $M(p\lambda)$ are in good agreement with tabulated $M(E\lambda)$ values.[18] Such agreement suggests that pion inelastic scattering can be used to measure and compare neutron and proton multipole matrix elements in cases where electromagnetic measurements do not exist.

In Table IV, the ratios obtained in the present experiment are compared with previous measurements. The most reliable of these is the mirror nucleus measurement for ^{42}Ca.[19] Values of $M(E\lambda)$ were measured for ^{42}Ca and ^{42}Ti. Assuming charge symmetry, $M(n\lambda)$ for ^{42}Ca is equal to $M(E\lambda)$ for ^{42}Ti, and the ratio R can be obtained from purely electromagnetic measurements. In

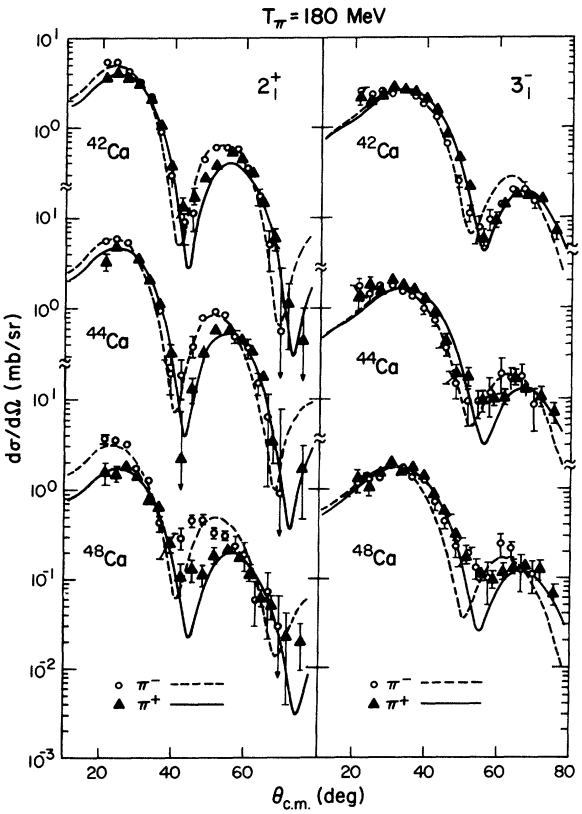

FIG. 3. Inelastic-scattering data and collective-model calculations.

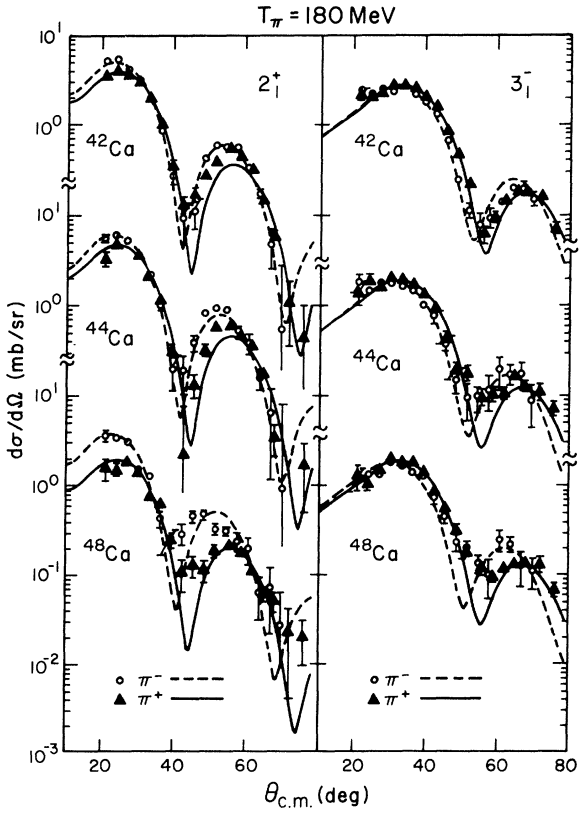

FIG. 4. Inelastic-scattering data with calculations using microscopic model form factors.

TABLE IV. Comparison of the ratios $M(n\lambda)/M(p\lambda)$ obtained by different methods.

State	Present data	Mirror[a] nuclei	(α,α')[b] electromagnetic	(p,p')[c] electromagnetic	Collective[d] model
^{42}Ca(2_1^+)	1.21(15)	1.35(13)	1.27(18)		1.10
^{44}Ca(2_1^+)	1.31(16)		1.28(23)		1.20
^{48}Ca(2_1^+)	2.38(33)		3.28(40)	2.58(39)	1.40

[a]Reference 19.
[b]Reference 1.
[c]Reference 2.
[d]The collective model prediction is N/Z.

general, good agreement is observed between present and previous measurements.

Two extreme models for the expected ratios are the collective model and the single-particle shell model. In the collective model, these 2_1^+ and 3_1^- states are viewed as equal amplitude ($\beta_n = \beta_p$) deformations or vibrations of the nuclear surface. Consequently, one would expect $R \simeq N/Z$, the approximate ratio of the surface neutron and proton densities. If excitations above the *fp* shell are ignored in the shell model, the 2^+ states should consist of $0-\hbar\omega$ excitations of the valence particles (neutrons), whereas the 3^- states should consist of $1-\hbar\omega$ excitation of the core nucleons (both protons and neutrons). Consequently, the 2^+ states should be excited only by neutron promotions $M(p\lambda) = 0$, whereas the 3^- states should be increasingly excited by proton promotions $M(p\lambda) > M(n\lambda)$, as the $f_{7/2}$ subshell is filled with neutrons which cause Pauli blocking of core neutron promotions.

The ratios for both the 2^+ and 3^- states lie between these extremes. An intermediate model[5] that incorporates both single-particle excitations and core-polarization effects (collective effects) has been successfully applied to ratios derived from (α, α') (Ref. 17) data.

VII. CONCLUSIONS

Neutron and proton multipole matrix elements for the excitation of low-lying collective states in the single closed-shell nuclei ^{42,44,48}Ca have been extracted from pion inelastic-scattering data at resonance energies. The proton matrix elements are in good agreement with electromagnetic matrix elements, and in general, the ratios of the neutron to proton matrix elements agree with previous measurements. These ratios for both the 2^+ and the 3^- states fall between those from a pure collective model and those from a single-particle shell model, indicating the need for a model that incorporates both valence-particle and core-polarization (collective) effects.

ACKNOWLEDGMENTS

The authors thank Professor J. S. Blair of the University of Washington for suggesting the possibility of an enhancement in π^+ vs π^- scattering to the 2^+ and 3^- collective states, because of Pauli-blocking effects in the calcium region. This work was supported in part by the United States Department of Energy and in part by the Robert A. Welch Foundation.

*Present address: Kirtland Air Force Base, Albuquerque, New Mexico 87117.
† Present address: New Mexico State University, Las Cruces, New Mexico 88003.
‡Present address: Los Alamos National Laboratory, Los Alamos, New Mexico 87545.
§Present address: University of South Carolina, Columbia, South Carolina 29208.
||Present address: University of Texas at Austin, Austin, Texas 78712.

[1]A. M. Bernstein, in *Advances in Nuclear Physics*, edited by M. Baranger and E. Vogt, (Plenum, New York, 1969), p. 325; and private communication.
[2]G. S. Adams, Th. S. Bauer, G. Igo, G. W. Hoffman, G. R. Smith, and M. Gazzaly, Phys. Rev. C 21, 2485 (1980).
[3]P. L. Hollowell, W. Bertozzi, J. Heisenberg, S. Kowalski, X. Maruyama, C. P. Sargent, W. Turchinetz, C. F. Williamson, S. P. Fivozinsky, J. W. Lightbody, and S. Penner, Phys. Rev. C 7, 1396 (1973).
[4]J. Heisenberg, J. S. McCarthy, and I. Sick, Nucl. Phys. A164, 353 (1971).
[5]V. A. Madsen, V. R. Brown, and J. D. Anderson, Phys. Rev. C 12, 1205 (1975); V. R. Brown and V. A. Madsen, *ibid.* 11, 1298 (1975).
[6]C. L. Morris, Phys. Rev. C 13, 1755 (1976).

[7]C. L. Morris, K. G. Boyer, C. Fred Moore, C. J. Harvey, K. J. Kallianpur, I. B. Moore, P. A. Seidl, S. J. Seestrom-Morris, D. B. Holtkamp, S. J. Greene, and W. B. Cottingame, Phys. Rev. C (to be published).
[8]H. A. Thiessen and S. Sobottka, Los Alamos National Laboratory Report No. LA-4534 MS, 1970; H. A. Thiessen *et al.* (unpublished).
[9]The program LOAF was written by Lester Eugene Smith, Physics Department, University of Texas at Austin, Austin, Texas 78712.
[10]C. M. Lederer and V. S. Shirley, *Table of Isotopes* (Wiley, New York, 1978).
[11]G. Rowe, M. Salomon, and R. H. Landau, Phys. Rev. C 18, 584 (1978).
[12]R. A. Eisenstein and G. A. Miller, Comput. Phys. Commun. 11, 95 (1976).
[13]L. S. Kisslinger, Phys. Rev. 98, 761 (1955).
[14]W. B. Cottingame and D. B. Holtkamp, Phys. Rev. Lett. 45, 1828 (1980).
[15]R. F. Frosch, R. Hofstadter, J. S. McCarthy, G. K. Nöldeke, K. J. van Oostrum, M. R. Yearian, B. C. Clark, R. Herman, and D. G. Ravenhall, Phys. Rev. 174, 1380 (1968).
[16]R. A. Eisenstein, D. W. Madsen, H. Thiessen, L. S. Cardman, and C. K. Bockelman, Phys. Rev. 188, 1815 (1969).
[17]A. M. Bernstein, V. R. Brown, and V. A. Madsen, Phys. Lett. 71B, 48 (1977).
[18]P. M. Endt, At. Data Nucl. Data Tables 23, 3, 547 (1979).
[19]A. M. Bernstein, V. R. Brown, and V. A. Madsen, Phys. Rev. Lett. 42, 425 (1979).